Fusion Engineering and Design 146 (2019) 1091–1095

Contents lists available at ScienceDirect

Fusion Engineering and Design

journal homepage: www.elsevier.com/locate/fusengdes

Maximizing JET divertor mechanical performance for the upcoming deuterium-tritium experiments

M.L. Richiusa*, D. Iglesias, G.F. Matthews, M. Porton, V.K. Thompson, Z. Vizvary

UKAEA-CCFE, Culham Science Centre, Abingdon, Oxon, OX14 3DB, UK

ARTICLE INFO

Keywords:
JET
Divertor integrity
ILW
D-T preparation
Synthetic plasma pulses
Experimental validation

ABSTRACT

The next D-T campaign will push the JET ITER-like wall to high divertor power and energy levels. During the 2016 campaign, Strike Point (SP) sweeping permitted relevant H-mode scenarios without exceeding the temperature limits imposed by JET Operation Instructions (JOIs). In the subsequent shutdowns, six outer divertor tungsten-coated 2D carbon fibre composite tiles were found to have inter-laminar cracks.

Here we describe the results of a 3D thermo-mechanical analysis aimed at understanding the origin of the cracks. A sensitivity assessment has been carried out on the temperature time-evolution of a realistic tile 3D model during high power pulses, both with fixed and sweeping SPs. Time and space-varying heat flux density loads on the divertor have been calculated using different techniques for reconstructing the power footprint. The results have been benchmarked against the temperature measurements by high resolution infrared diagnostic systems.

The study confirmed the source of the cracks and their localization in the upper part of the tile, giving inter-laminar tension higher than the Ultimate Tensile Stress. Plasma input power, radial location of the SP and sweeping amplitude play an important role on the stress field whose maximum value strongly depends on the SP location. Their influence on the maximum stress value has been investigated and optimized to maximize the performance of divertor tiles without exceeding the limits on input energy and maximum surface temperature imposed by the JOIs.

1. Introduction

The Joint European Torus (JET) is the world largest tokamak and the only one able to operate with tritium. The upcoming experimental campaign will be of great importance for ITER, foreseeing the exploration of isotope effects on transport, confinement, L-H mode transition, pedestal physics, and plasma-wall interaction by operating with H_2, D_2 and T_2 using the ITER-Like Wall (ILW). Going towards its second D-T campaign (DTE2), JET will be pushed to much higher power levels. Every operational scenario must comply with the JET Operating Instructions (JOIs) [1] that define limits on JET experiments to prevent excessive heat loads on Plasma Facing Components (PFCs). As the JET divertor targets are inertially cooled, these limits are imposed on divertor tile input energy (i.e. plasma input energy reduced by the plasma radiative energy) and on maximum surface temperatures.

The 2015-16 JET experimental campaign, enhancing the High-performance plasma scenario in preparation for the DTE2, was characterized by plasma pulses performed by sweeping the Strike Point (SP) [2]. This technique permitted high power pulses for longer without exceeding the temperature limits on the divertor surface where the hot exhaust plasma streams along the open magnetic field lines, Fig. 1. Following the numbering of the tiles indicated in Fig. 1, the divertor targets holding the SP are the inboard vertical (3) and horizontal (4) tile rows and the outboard horizontal (6) and vertical (7) tile rows near the pumping duct entrance. After the installation of the JET ILW [3], the divertor tiles are all made of 2D Carbon Fibre Composite (CFC) covered by a thin layer of tungsten (˜20 [μm]) except the central row (5) that is made of bulk tungsten.

Although the last campaign was one of the most successful for improving plasma physics understanding, cracks were subsequently found in six Tile 6s. The cracks extended radially along inter-laminar planes. Initially it was not known whether the cracks were superficial (tungsten coating delamination damage) or extended into the bulk material of the tile (Fig. 2, detail pointed out by red rows). Sometimes the cracks were accompanied by beryllium droplets on the tungsten upper surface.

Tile 6 integrity is fundamental for DTE2 scenario as it is the most requested target since it allows to better handle pulse power by sweeping the SP, improving at the same time the cryo-pump efficiency.

* Corresponding author.
E-mail address: lorena.richiusa@ukaea.uk (M.L. Richiusa).

https://doi.org/10.1016/j.fusengdes.2019.02.013
Received 28 September 2018; Received in revised form 22 January 2019; Accepted 5 February 2019
Available online 15 March 2019

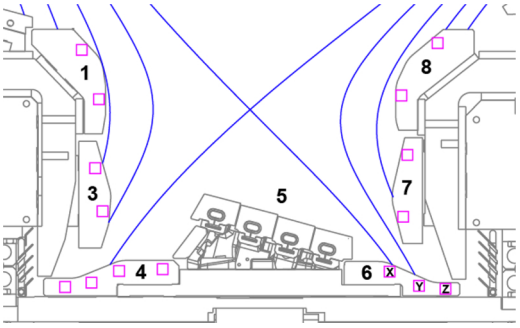

Fig. 1. Cross section of the JET divertor after the ILW installation showing tile numbers.

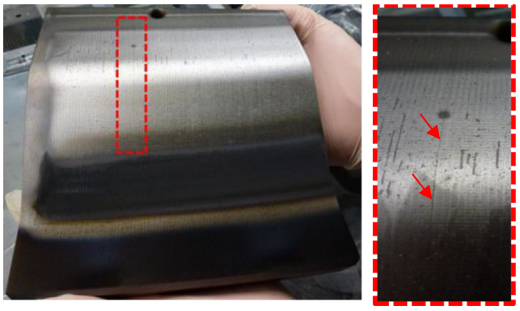

Fig. 2. Cracking damage observed on Tile 6.

Risks connected to its failure are: 1. release of particle impurities (e.g. tungsten, carbon) into the plasma; 2. tritium absorption by CFC; 3. tile erosion on the high-flux side, i.e. the part of the tile closer to the inboard side where the magnetic field is stronger. In addition, previous studies on the failure of the tie rods designed to hold the CFC plies together showed that they don't prevent tile cracking since the tile itself is stiffer than the tie rod [4], and this poses a risk of a combined failure leading to complete tile breakage inside the machine. To reduce the risk of further failure during the upcoming JET restart phase, the cracking damage has led to a detailed investigation of the thermo-mechanical behavior of Tile 6. The study, based on modelling the real-time heat load acting on the tile surface, aims to find a relation between the tile stresses and the range of plasma parameters related to this phenomenon.

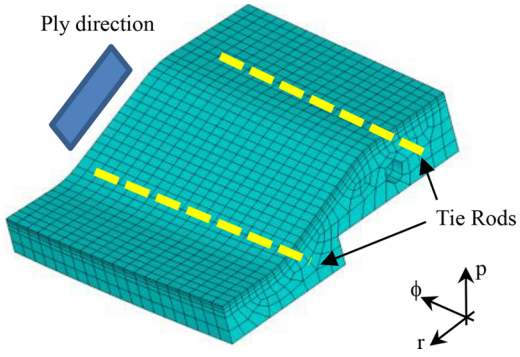

Fig. 3. Tile 6 FE model.

2. Characterization of the failure mechanism

The risk of delamination of tungsten coating due to the thermally-induced carbidisation and consequently embrittlement of the interface requires real-time protection during operations. Infra-Red (IR) thermography based on image diagnostics (IR Cameras) has been installed and upgraded [5] for building the Vessel Thermal Map (VTM), detecting hot spots on PFCs and, if necessary, terminating pulses. In this study, the surface temperature value measured by IR cameras with high dynamic range (14 bit) [6] will be used as a reference for validating the results.

The main issue is the calculation of a realistic heat load profile on the divertor tile. Using Finite Element (FE) modelling for transient thermo-mechanical analyses, the study can be divided into two phases characterized by two different assumptions on computing the realistic heat load on the tile surface:

- Phase 1: capturing of the failure modes using IR-derived heat load profiles calculated through inverse analyses [7] and identification of the main machine parameters affecting the behavior of the tile.
- Phase 2: creation of synthetic pulses linked to the next C38 campaign using a convolution of a Gaussian with an exponential profile (Eich's function) for calculating the power footprint on the tile surface [8].

2.1. Geometry, FE model and materials

The Tile 6 FE model is shown in Fig. 3. Tie rods are not needed in this work according to what explained in §1 (for a detailed investigation of this issue see [4]). The tile is made of CFC plies stacked along the toroidal direction (φ-axis in Fig. 3), covered by 20 [μm] tungsten layer. The model includes the temperature dependence and orthotropic nature of the CFC. The thinner tungsten layer is not modelled as the mechanical response of the tile under pulse heat load is entirely determined by bulk CFC.

From the structural point of view, Tile 6 FE model is constrained in such a way to prevent any rigid body motion allowing, at the same time, the tile to expand unhindered whilst keeping the model determinate.

2.2. Phase 1: cracking damage investigation

Table 1 shows the pulses of interest run during the last campaign with an outer SP located on Tile 6 surface. Two fixed SP pulses (denoted with the subscript 'f') and two swept pulses (denoted with the subscript 's') have been chosen.

Applying IR-derived heat loads on the tile surface and a Toroidal Wetted Fraction (TWF) of 70%, a good agreement (within 15%) between the experimental data and the modelled surface T_{MAX} time-evolution has been obtained for all the pulses (Table 2). The results obtained in Phase I (in terms of T_{MAX} and σ_{MAX} vs time) will be used as a reference for the validations made in Phase II.

In the following, the results related to JPN:92025 are reported in terms of comparison between $T_{MAX,IR}$ and $T_{MAX,FEM}$ time-evolution

Table 1
JET Pulse Numbers (JPN) of interest run during the last JET campaign (M15-02 scenario [9]).

JPN	Experiment	I_p [MA]	B_T [T]	SP [m]	NBI [MW]	Δt [s]
89297$_f$	M15-02 Hybrid scenario for D-T	1.9	1.4	~0.24	13.0	7.0
90287$_f$	M15-02 Hybrid scenario for D-T	1.9	1.4	~0.24	13.4	7.5
90271$_s$	M15-02 Hybrid scenario for D-T	2.4	2.8	0.24-0.27	17.0	7.5
92025$_s$	M15-02 Hybrid scenario for D-T	2.5	2.9	0.24-0.27	23.5	5.5

Table 2
Summary of experimental and FEM data for each pulse for Tile 6.

JPN	Thermal Results				Mechanical Results
	Experimental Data		FEM Data		
	T_{MAX} [°C]	$E_{th,DIV}$ [MJ]	T_{MAX} [°C]	$E_{th,DIV}$ [MJ]	Toroidal stress [MPa]
89297$_f$	873	32.02	794	29.76	6.05
90287$_f$	1039	36.48	848	36.48	7.61
90271$_s$	1017	50.84	918	48.00	7.32
92025$_s$	1107	39.82	936	33.83	6.76
92025$_s$**_1.12***	1107	39.82	1194	38.40	8.05

* same JPN:92025 whose thermal energy input the divertor has been incremented by 12%.

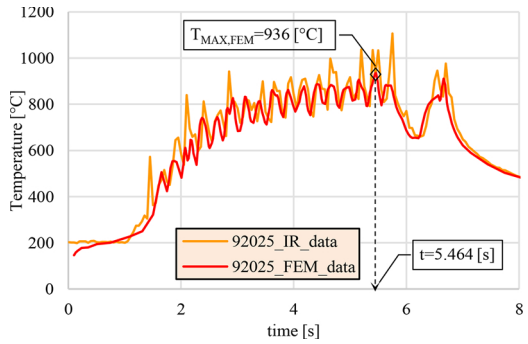

Fig. 4. Comparison between experimental T_{MAX} and modelled T_{MAX} – JPN: 92025. $T_{MAX,FEM}$ maximum value is reached at 5.464 [s] (red line). (The reader is referred to the online version of the paper for any reference to the colors in the figure).

trends (Fig. 4) with temperature and stress contour plots (Fig. 5) related to the time instant in which the $T_{MAX,FEM}$ reaches its maximum value. These results are representative of the results obtained for all the pulses analyzed.

2.3. Phase 1 preliminary conclusions

The results show the synergic effects of two large thermal gradients: radial lateral and vertical (i.e. along the r and p directions, respectively, indicated in Fig. 3). The radial lateral gradient (˜9.4 [°C/mm]) on the top surface between the central area intersected by the SP and the cooler inner and outer sides (Fig. 5a) leads to central compression and tension on the sides (Fig. 5b). These side tensile stresses tend to delaminate the tile, trying to pull away the CFC plies along the toroidal

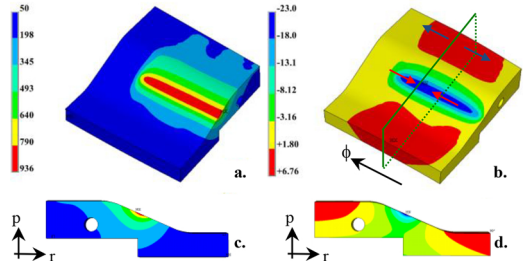

Fig. 5. ***(a.)*** Time-instant thermal field [°C] (t = 5.464 [s]) and ***(b.)*** related stress field distribution [MPa] along the toroidal direction (φ-axis, with blue and red arrows representing tensile and compressive stresses, respectively) on Tile 6 for JPN: 92025 swept pulse. An overview of the temperature and stress field distribution along Tile 6 toroidal cross section is given in ***(b.)*** and ***(c.)***, respectively. (The reader is referred to the online version of the paper for any reference to the colors in the figure).

direction. They are located exactly where the cracks appeared (Fig. 2) and of magnitude consistent with local failure (the inter-laminar tensile strength is about 7 [MPa]). This effect is amplified by the higher vertical thermal gradient (˜20 [°C/mm]) which causes the tile bending about the r-axis (of the machine) with increased tension on the top surface. The difference in temperature between the shadowed and the heated area gives a contribution to the cracking initialization, being the bending effect produced by the vertical thermal gradient the main enhancer of cracking damage. Therefore, the cracks appear radially as a result of large stresses in the toroidal direction which is the weakest direction of the tile. The shadow effect does cause stresses in the radial direction, but the tile is able to resist these due to the 2-D reinforcement.

Previous analyses [4] performed on Tile 6 equipped with tie rods showed that, even if the tie rods slightly help in limiting the thermal expansion of the tile along the toroidal direction, they don't help in limiting the bending of the tile since they are less stiff than the tile itself and, being installed without no preload, they play a very little role in preventing tile cracking. So, they are stretched by the tile that is expanding quicker than the tie rods since the heat travels along the CFC planes first and only when the temperature of the tile starts to even among all the plies the tie rods experience a relaxation of the stress because they start to expand but, still, they continue being stretched by the tile itself that determines the whole behavior of the system (Tile 6 + tie rod).

The relation between these stresses and the tile thermal energy will be discussed later.

3. Phase II: sensitivity analysis using synthetic pulses

The limited number of high-resolution pulses, the good agreement with the IR data obtained in Phase I and the need to investigate the relation between stress field and operational parameters (SP position, sweeping amplitude) led to a sensitivity analysis based on *synthetic* pulses.

Synthetic pulse: discharge related to the up-coming JET C38 campaign simulated imposing constant values of Neutral Beam Injection (NBI), Ion Cyclotron Resonance Heating (ICRH) and Ohmic heating power for 6-7 seconds and using Eich's function for the heat load profile (engineering power footprint) by imposing engineering and plasma parameters (B_t, I_p, n_e, f_{ELM}) [10].

What is important for the present study is an estimation of the average bulk effect of all the power loads acting on the tile, therefore the power footprint takes into account temporal averaged effects of inter-ELMs and ELMs without analysing separately the transient thermal excursions due to ELMs. It is worth pointing out that, previously to the study described here, the effects of ELMs on the oscillating stress trend were analysed in detail using IR experimental data. The heat flux inferred from thermography with sampling frequencies up to 20 [kHz] was applied to a FE model of an isolated probe for investigating the local stress due to alternating surface heat gradient obtaining a stress trend that follows the heat flux frequency with slight variations always below 1 [MPa]. This outcome justifies the use of the time-averaged (ELM + inter ELM) heat flux distribution at the tile surface. The function of the engineering power footprint used for resolving ELM and inter-ELM effects is explained in detail in [10].

The methodology uses three main steps summarized in Table 3.

Step I validates the power footprint against IR-derived heat flux. Step II validates the swept pulses of Table 1 recreated synthetically against IR-derived data. Step III is independent of existing experimental data and studies the effect of operational parameters on the tile mechanical stress using synthetic pulses.

3.1. Step I: engineering footprint vs IR-derived heat flux

The two swept pulses of Table 2 have been run using the

Table 3
Summary of the methodology steps.

Methodology			
Rationale	Stages	Data	Outcome
Validation against existing discharges	Step I	*Read from JET database:* ● B_t, I_p, n_e, f_{ELM} ● NBI, ICRH, Ohmic power	engineering footprint vs IR-derived heat flux (checks in T_{MAX} and σ_{MAX})
	Step II	*Imposed constant values:* ● B_t, I_p, n_e, f_{ELM} ● NBI, ICRH, Ohmic power	synthetic swept pulses against IR-derived data (checks in T_{MAX} and σ_{MAX})
Synthetic pulses	Step III	*Imposed constant values:* ● B_t, I_p, n_e, f_{ELM} ● NBI, ICRH, Ohmic power	JET C38 experimental campaign synthetic pulses and sensitivity analysis

engineering power footprint [10] for modelling the power density on the tile surface. Compared to the results using IR-derived heat loads (Phase I) taken as reference, the maximum error on T_{MAX} and σ_{MAX} is about 13% and 38%, respectively. Overall, the power footprint gives a good estimation of the heat load, but it needs to be refined during the up-coming restart phase. Main limitations: an average value of n_e (1.4E + 20 [m^{-2}]) and f_{ELM} (40 [Hz]) is imposed during the pulse.

3.2. Step II: synthetic pulses vs IR-derived data

The two swept pulses of Table 2 have been recreated synthetically using as heat load the power footprint validated in Step I and imposing from scratch the plasma power input, preserving the experimental thermal energy indicated in Table 2. The power going into the SOL has been estimated according to the following conservative assumptions: 1. NBI and ICRH power input assumed constant for 6–7 seconds; 2. constant radiated power loss by fraction of 30% ($P_{RAD} = 0.3 \cdot P_{TOT,plasma}$). The power density on the divertor surface estimated through forward analyses [7] has been applied in the thermo-mechanical FE model giving promising thermal and stress results in comparison with the ones obtained in Phase I for the relevant pulses. These results will be reviewed during the JET experiments. The error obtained on T_{MAX} and σ_{MAX}, whose maximum value is about 1000 [°C] and 11 [MPa], respectively, is of the same order of magnitude as before. Having validated the procedure against existing pulses, the study has been carried on without relying on existing experimental data.

3.3. Step III: synthetic pulses and sensitivity analysis

This step creates new pulses for Hybrid and Baseline scenarios planned for the next JET campaign. Two different power levels have been set, according to the availability of the NBI (30 and 40 [MW]), as well as different values for SP location and sweeping amplitude. The sensitivity analysis examines how the last two variables affect the thermally-induced stress for a fixed power level. For every SP location (2.85, 2.90, and 2.95 [m] major radii – SP_1, SP_2, SP_3, respectively, in Fig. 6), two different sweeping amplitudes have been considered (0.03-0.06 [m], respectively indicated with yellow and red markers in Fig. 6).

The sensitivity analysis confirmed the proportionality between Tile 6 toroidal stress and thermal energy input. Figs. 7 and 8 show the results, in term of T_{MAX} and σ_{MAX} time-evolution, respectively, of the 40 [MW] pulse with different combinations of SP location and sweeping amplitude. A change in SP location can reduce the stress value by up to 60% when the SP is moved outboard and only slightly affects the T_{MAX}. In contrast, change in the sweeping amplitude has beneficial effects in decreasing the T_{MAX}.

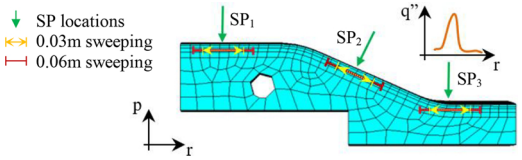

Fig. 6. Graphical summary of the main parameters involved in the sensitivity analysis.

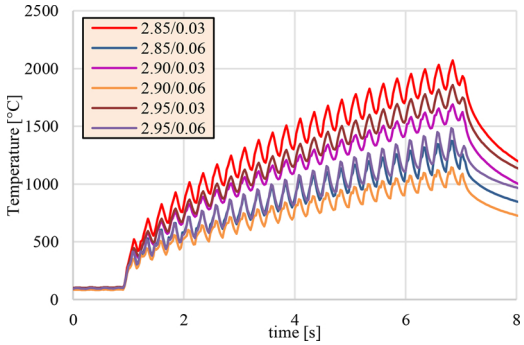

Fig. 7. Tile 6 T_{MAX} time-evolution for a 40 [MW] plasma pulse at different SP locations and sweeping amplitude.

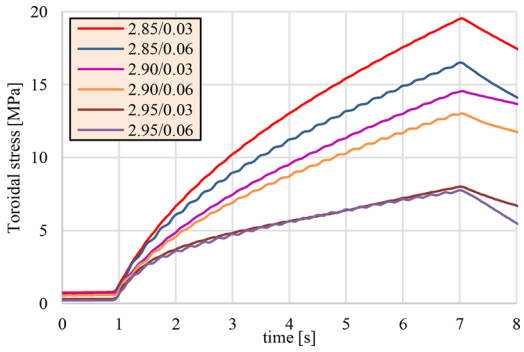

Fig. 8. Tile 6 σ_{MAX} time-evolution for a 40 [MW] plasma pulse at different SP locations and sweeping amplitude.

The sweeping doesn't produce big oscillations in the stress trend, as it does instead in the temperature trend. Therefore, it is worth pointing out that at 4 [Hz] sweeping frequency, the tiny fluctuations in the stress trend are not a matter of concern for fatigue issue. The stress evolution mainly follows monotonically the increase in temperature without visible fatigue cycle trend in their evolution.

4. Conclusions

The cracks found in six JET divertor Tile 6s during the 2017 shutdown have led to an investigation of the thermo-mechanical behavior of Tile 6 under plasma pulses. The study has identified the main operational parameters that can be monitored to avoid further cracking during the upcoming campaign (Fig. 6). Preliminary conclusions show

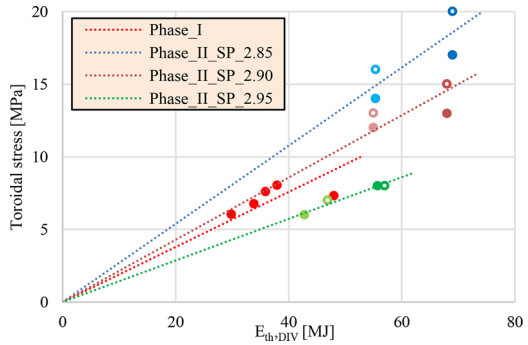

Fig. 9. Toroidal stress against Tile 6 thermal energy. Each line indicates three SP positions and the associated pulses with different sweeping amplitude (0.03 and 0.06 m represented using open and closed circle markers, respectively) and different input power levels (30 and 40 MW, indicated with light and dark color for the same sweeping amplitude, respectively). (The reader is referred to the online version of the paper for any reference to the colors in the figure).

the dependency of thermal stress on the energy discharged onto the tile through the SOL, therefore suggesting increasing stress values as the plasma power input increases (red line in Fig. 9 representing pulses of Table 2 with different power levels but same SP location. The dots following the red line are characterized by a slight increase of plasma input power; the red dot below the line has a lower input power and a longer duration).

The sensitivity analysis relevant to the next campaign has underlined that the dominant effect on tile stress is due to the SP position, as Fig. 9 clearly shows. For the most outboard SP at 2.95 [m] (green line), the sweeping amplitude doesn't have such a significant influence compared with the inboard case (2.85 [m]). For the 2.95 [m] case, about 17% of the SOL power is released in Tile 7, so the energy sharing between Tile 6 and Tile 7 can reduce the stress by about 40–60%. The sweeping amplitude has influence on the T_{MAX} but very slight influence on the σ_{MAX}.

The assumptions and the limitations of the methodology (which will be validated during JET operations) are conservative (T_{MAX} values are higher than expected). This does not affect its goal because it has been useful for understanding the relation among stress, SP location, sweeping amplitude and plasma power levels and in identifying the SP location as the most critical parameter.

Cracks cannot be avoided at energy levels above about 35 MJ, but the tie rods will prevent complete tile failure and allow for remote maintenance. The rods themselves are also vulnerable to failure through fatigue and so their integrity is managed through rationing of high energy pulses.

Acknowledgments

This work has been carried out within the framework of the Contract for the Operation of the JET Facilities and has received funding from the European Union's Horizon 2020 research and innovation programme. The views and opinions expressed herein do not necessarily reflect those of the European Commission.

References

[1] D. Stork, et al., Fusion Eng. Des. 47 (1999) 131.
[2] S.A. Silburn, et al., Phys. Scr. 2017 (2017) 014040.
[3] G.F. Matthews, et al., Phys. Scr. 2011 (2011) 014001.
[4] P. Bunting, Tile 6 Tie Rod Fatigue Analysis, IVER_UM_1500_D014, November (2015).
[5] G. Arnoux, et al., Rev. Sci. Instrum. 83 (2012) 10D727, https://doi.org/10.1063/1.4738742.
[6] I. Balboa, et al., Rev. Sci. Instrum. 83 (2012) 10D530, https://doi.org/10.1063/1.4740523.
[7] D. Iglesias, et al., Digital Twin Applications for the JET Divertor, October (2017).
[8] T. Eich, et al., Nucl. Eng. 53 (2013) 093031.
[9] M.J. Mantsinen, et al., European Physical Journal Web of Conferences 157 (2017) 3032, https://doi.org/10.1051/epjconf/201715703032.
[10] V. Riccardo et al., Power footprint definition for JET divertor protection, EUROfusion WPJET1-PR (16) 14684.